Ball burnishing effect on deep residual stress on AISI 2038 and AA2017-T4

Abstract

Ball-burnishing induces compressive residual stresses on treated materials by the effect of plastic deformation. The result is an increase in the fatigue life of the treated part, retarding the initiation of cracks on the surface. Compressive residual stresses have been previously measured by X-ray diffraction near the surface, revealing considerable high values at the maximum analyzed depth, in relation to other finishing processes such as shot peening. However, the maximum analyzed depth is very limited by using this technique. In this paper, the incremental hole drilling technique is tested to measure residual stresses, being able to reach a 2-mm measuring depth. To that objective, a commercial strain gage is used and calibrated using finite element model simulations. A second FEM based on material removal rate is developed to obtain the equations to calculate the strain release through incremental hole drilling. Finally, residual stresses are measured experimentally with that technique on two different materials, confirming that ball-burnishing increases the compressive residual stresses in layers up to 0.5 mm deep for the testing conditions, which is a good response to industrial needs. The method proves to be suitable, as a simple and inexpensive way to measure the value of these tensions.

Keywords: burnishing, residual, stresses, incremental, hole, drilling, aluminum, steel, finite, element, method,

1. Introduction

Current industry requires high quality finishing of mechanical parts to increase their fatigue resistance and achieving a low friction ratio. In this context, the relevance of

surface integrity is basic, so the development of finishing processes has turned one of the main drivers of industrial innovation worldwide. In effect, they are responsible for

the final residual stress state, hardness and surface roughness conditions of parts, factors on which fatigue life is dependent. These specific conditions can be obtained through several processes, such as burnishing, shot peening and electro-polishing. Shepard et al. (2003) [1] analyzed the fatigue response on aeronautical Ti-6Al-4V specimens. These pieces were subjected to three processes: ball-burnishing, shot peening and electro-polishing. A comparative analysis of their surface roughness was performed. Ball burnishing resulted in the lowest surface roughness (average roughness $R_a \approx 3$ µm), while electro-polishing and shot peening resulted in $R_a \approx 17$ µm and $R_a \approx 85$ µm, respectively.

Ball-burnishing is considered a cold-working process, during which, elastic-plastic deformation is produced on the workpiece because of the constant force transmitted by the tool [2]. This operation is developed using a tool attached to a CNC machine, applying a certain calibrated force to a sphere. The sphere glides over the workpiece area, deforming the peaks of the surface irregularities and flattening the roughness profile, producing a much more regular surface. The process is known for its positive effects on surface integrity. El-Axir et al. (2008) [3] proved the decrease in average surface roughness of 2014 aluminum specimens, as the level of cold work was increased by higher burnishing force and number of passes. These positive results have also been proved on concave and convex surfaces, as show Travieso-Rodriguez et al. (2011) on steel and aluminum workpieces [4]. Secondly, surface hardness is enhanced by burnishing due to cold work deformation, as show Prévey et al. (2002) [5] on Ti-6Al-4V specimens. The same authors conclude that stress introduced by burnishing reach compressive values at depths higher than 1 mm. That result is confirmed by other authors, such as Zhang et al. (2011) [6]. As a consequence, wear resistance of burnished materials is improved, which shows the comprehensive effects of burnishing as a

finishing process (Hassan et al., 1999) [7], and a longer lifespan of industrial components can be expected, as explained by Hariharan & Prakash (2001) [8].

Many ball-burnishing tools exist in the market, such as the ones commercialized by Mech-India Engineers [9] or Ecoroll AG Werkzeugtechnik [10], and the one developed and patented by Travieso-Rodriguez et al. [11].

The ball burnishing process has extensively been the object of research activities tackling with the optimization of process parameters and the development of theoretical models. For instance, Rodriguez et al. [12] published a model to optimize ball-burnishing parameters, taking surface roughness and residual stresses as response variables. Recent studies, introduce the assistance of vibrations in the process, revealing a relevant improvement of results. Zhao et al. (2016) [13] applied ultrasonic multi-roller burnishing on Ti-6Al-4V specimens, observing a decrease of the material flow stress, which in turn allows lower forces to be applied to achieve the same cold work deformation and residual stresses. Travieso-Rodriguez et al. (2015) [14] concluded that a ball burnishing process assisted by a 2-kHz vibration allows to achieve similar results in one pass, with regards to five passes of the conventional process. The results are confirmed on carbon steel specimens (Travieso-Rodriguez et al., 2015) [15].

Residual stresses can be measured through different methods, which can be classified according to the way they interact with the tested material. A comprehen sive

review of residual stress measurements methods is explained at Withers and Bhadeshia (2001a,2001b) [16,17]. Methods involving material loss are known as destructive methods. An example of a totally destructive method is explained by Garcia-Granada [18,19]. If the material is locally removed, although not compromising the structural integrity of the component, these methods are referred to as semi-destructive. Two good examples are deep hole drilling and incremental hole drilling [20,21]. In contrast, non-

destructive methods do not affect the integrity of the tested part, using diffraction of neutrons according to Maawad et al. [22] or X-Ray diffraction [14,15,23-25] to estimate near-surface residual stresses. The major drawback of this diffraction method is the low depth to which compressive residual stresses measurements can be performed. For this reason, incremental hole drilling (IHD) is tested as an alternative method to measure residual stresses in burnished specimens, able to reach deeper layers.

The IHD method is a well-known and common technique to evaluate residual stresses at any position of the surface of a workpiece up to a depth around 2 mm [26,27]. The maximum measurable depth depends on the selected strain gage rosette, and is defined at the E837-08 ASTM standard [28]. There are many ways to analyze strain release during incremental hole drilling, as summarized by Ajovalasit et al. [29]. In order to estimate the error of measuring residual stresses near the yield stress value, finite element simulations can be carried out in order to adapt the testing parameters to that condition [30-32]. Gharbi et al. [33] showed the effect of the ball-burnishing force on residual stress on the surface of AISI 1010. Zemčík et al. [34] measured the same on EN 10132-4 specimens. Abdulstaar et al. [35] showed the fatigue improvement on Al6082 for both shot peening and ball-burnishing with compressive residual stresses up to 0.5 mm below the surface but without describing the directionality of residual stresses and the method used to measure them.

This paper has two objectives. The first one is to demonstrate that ball-burnishing is a successful process in introducing compressive residual stresses in layers at a few millimeters below the surface. This verification is basic to validate the ball-burnishing process to treat industrial parts subjected to fatigue working regimes during their lifespan.

The second one is to validate the incremental hole drilling method to measure compressive residual stresses of burnished parts, by comparing it to X-ray diffraction results available and developed by other authors [14,15]. IDH has not been extensively applied to assess the effects of ball burnishing at deep layers of the material because its application is more difficult than X-ray diffraction. Nevertheless, it is a cheaper method, and allows to perform measurements at higher depths of the treated part, that is, to assess in a more comprehensive way the effects of plastic deformation derived from ball burnishing.

2. Materials and methods

Four specimens of AA2017-T4 aluminum and four of AISI 2038 steel were tested. The most relevant properties for both materials are shown in Table 1. The samples were prepared through an initial face milling using a CNC milling machine and an 80-mm diameter plate tool mill with five inserts. Cutting parameters were 3000 min^{-1} of cutting speed, a feed rate of 1000 mm/min and 0.5 mm of depth of cut. After that, they were subjected to a ball-burnishing operation, using the tool designed by Gómez-Gras et al. [36] (Fig. 1), equipped with a 10-mm diameter burnishing ball. Different forces were applied for both treated materials, being 90 N the nominal force for aluminum and 110 N for steel. The feed velocity was 600 mm/min and 1 pass was performed along every burnishing path. These values were selected based on the results obtained in different experimental research, according to Travieso-Rodriguez et al. [6].

Table 1

Figure 1

The burnished specimens were then equipped with a strain gage rosette to measure the induced residual stresses effect of the burnishing force. The chosen rosette

was the 1-RY21-3/120 (RY21 henceforth) from HBM. For this rosette, the mean diameter of the strain gages is D=13 mm, larger than the defined as type A in the ASTM E837-08 standard [28]. The main reason of using such a large rosette is because it allows to measure residual stresses down to deeper layers of the material. The minimum recommended thickness of the specimen is 1.2D=15.6 mm, condition satisfied by using 40-mm thick specimens. Strain gage ε_{1x} was always aligned with the ball-burnishing direction, as shown in Fig. 2A. The rosette was then connected to a Spider 8 data acquisition device.

Figure 2 A), B)

To perform the burnishing experiments, a simple CNC was programmed and implemented in an Odisea CNC machine operated by a Fagor 8055 controller, as shown in Figure 2B. This CNC machine was used to perform the stepped drill required for the measurement, using a 5-mm diameter drill, inside the admissible interval (4.751, 5.385) defined at the ASTM standard, dependent of the rosette diameter. The incremental drilling procedure is described in the standard as a process in which successive drills are performed until reaching the maximum depth, increasing each time the depth of cut by 0.13 mm. In this case, lower steps of 0.05 mm were used to obtain a more accurate strain relaxation profile as a function of the depth. Such small increments were also used in FEM calibration of parameters to obtain residual stresses from released strains.

Rosette RY21 is not calibrated in the ASTM E837-08 standard, but the standard states that calibration matrixes for other rosettes can be obtained by adjusting D and the hole diameter to the main parameters. In this case, the parameters applied to obtain non-uniform residual stress distributions with those given for a rosette of D = 5.13 mm, with a hole diameter of 2 mm and steps of 0.05 mm. Following this rule, the maximum measured depth was 2.534 mm, coinciding with the objective range of residual stresses

to be measured. The final hole depth specified in the standard should be around $0.4D$ = 5.2 mm for thick workpieces with uniform residual stresses. In order to get a proper matrix component for RY21 finite elements simulations were carried out.

Experimental corrections through Finite Element Models

This paper shows two different finite element models to validate the experimental drilling method for burnished parts. The first one, as already explained, allows to calibrate the RY21 rosette, as it is not calibrated at the reference ASTM standard. The objective of the second one is to correct the eccentricity between the drill and the center of the rosette. This correction is necessary because too high deviations could lead to erroneous results.

Finite element simulation to calibrate Rosette RY21

The strategy of using a large strain gage rosette in combination with small depth increase between drilling steps to obtain deeper and more accurate residual stresses, requires the generation of a corrective matrix of coefficients. This approach was already taken by Schajer and Steinzig, and Montay et al. to measure residual stress of shot peened parts [37-38], and Sedighi and Mahmoodi for angular rolling [27]. Niku-Lari et al. [39] found the calibration matrix for a RY21 rosette using steps of 0.01 mm and 4 and 5-mm drills. Unfortunately, matrix parameters were not provided in the paper.

Firstly, a simple simulation applying a constant pressure, p, to calculate a_i is required. A second simulation applying a cyclic pressure $p \cdot \cos(2\theta)$ and shear pressure $p \cdot \sin(2\theta)$ are required to obtain b_i. These simulations are performed for each drilling step. This means that, to achieve a total depth of 5 mm in steps of 0.05 mm, 100 geometrical models must be created, and two different simulations must be run for each one.

To perform this iterative calculation, a parametric model was built in SOLIDWORKS. 200 simulations were executed, and results were collected through a link between the parametric model in SOLIDWORKS and a datasheet in EXCEL. Equation (1) shows an expression given by Montay et al. [38], with a correction for depth step by Sedighi and Mahmoodi [27] and Niku-Lari et al. [39] and a correction in strain gages definition by Xiao et al. [40].

$$a_{in} = \frac{2E}{(1-v)} \frac{U_2 - U_1}{2p(r_2 - r_1)\Delta h} \quad (1)$$

$$b_{in} = 2E \frac{U_2 - U_1}{2p(r_2 - r_1)\Delta h} \quad (2)$$

where U are the values of nodal displacement, r_1 is the minimum radius position, r_2 is the maximum radius position. In the case of the RY21 rosette, r_1 = 5 mm and r_2 = 8 mm, which means that $D = r_1 + r_2$ = 13 mm, as explained above. Subindex i, refers to the ith layer, out of a total of n layers throughout the total thickness, Δh.

Fig. 3 shows the parametric model drawn in SOLIDWORKS, including the radius of the drilling hole, r_h = 2.5 mm, and an increase step of 0.05 mm between layers.

Figure 3

The mesh size was set to 0.05 mm at the edge of hole, evolving to 0.5 mm at remote points. The model was composed of 202,064 tetrahedral solid elements. Once all the simulations were carried out, parameters were obtained and fitted to a curve as a function of the drilling depth. These fitted curves would eventually allow using different steps to speed up the IHD measurement process. Parameters and curve fitting are shown in figure 4 for the first 2 mm of depth to obtain a good curve fitting in the area where residual stress measurements need to be assessed.

Figure 4

The estimation of a and b obtained from this FEM model is in agreement with those reported by similar studies [27-29,38-40]. Nevertheless, the ASTM standard suggests that all hole and stress depths should be multiplied by 13/5.13 to take into consideration the change in the rosette diameter, and also by $(5/2)^2$ to take into consideration the change in the drill diameter. Such correction is plotted in Fig. 4 to show that when different rosettes are considered, this approximation is not good enough, as there are many parameters changed from the calibrated data.

Residual stress experimental validation, through 4-point bending test

A device has been designed to introduce 4-point bending loads on aluminium plates (65x59x5 mm), in order to validate experimentally the measurement procedure, proposed in the previous subsection (Fig. 5).

Figure 5

Two forces P are applied on the specimen trough each screw of the device. The consequent stress and deflection at each specimen section can be calculated by eqs. 3 and 4 respectively.

$$\sigma(x)_{a<x<L-a} = \frac{Pah/2}{I} = \frac{6Pa}{bh^2} = 0.048P[\text{MPa}] \quad (3)$$

$$\delta(x)_{a<x<L/2} = \frac{Pa}{6LEI}(L-x)[L^2-(L-x)^2-(a)^2] + \frac{Pa}{6LEI}x[L^2-x^2-a^2] \quad (4)$$

Where a is the loadspan, h the height; b is the width; L is the length of the specimen and I is the moment of inertia.

The maximum force to be applied to achieve the yield stress is given by eq. 5.

$$Pmax = \frac{\sigma_x b h^2}{24\, a} = 4447.9 \text{ N} \quad (5)$$

Eqs. 3 and 4 can be verified using simulations of the 4-point bending device where 1000 N forces are applied. 48 MPa of stress are expected. Fig. 6 shows the comparison between experimental and theoretical stress results, demonstrating that the used method is adequate although a slight deviation is observed in the first 0.3 mm.

Figure 6

Finite element simulations of incremental hole drilling

A second application of FEM simulations is necessary to estimate the errors introduced by the drill eccentricity with respect to the rosette center, as reported by several autho rs such as Svarıcek and Vlk [41], Ghasemi, A. R.; Mohammadi, M. [42] and Schuster, S.; Gibmeier, J. [43]. This step is recommended, for the standard sets a maximum eccentricity of $0.004D = 0.052$ mm.

A simulation of the material removal process is performed to obtain the released strains as during the IHD measurement. The main objective is to validate *a* and *b* parameters with the real measured residual stresses. The FEM is developed using ABAQUS, comprising a first step to introduce a residual stress in the specimen, and subsequent phases modelling the IHD measurement itself. The initial coarse mesh size was set to 0.5 mm in all directions, with depth steps of 0.5 mm up to a maximum depth of 5 mm. In order to drill 2 mm just four points at depths of 0.5, 1.0, 1.5 and 2.0 mm are obtained. Finally, the fine mesh size was set to 0.05 mm at each layer to be removed during the drilling operation. In that way, the first layer of 0.05 mm was removed in

step 2. Each layer was removed in subsequent steps, until a maximum 2 mm depth corresponding to step 41. At a distance of 0.5 mm far from the edge of the hole, a transition to a 0.5 mm mesh was established, thus creating 82032 solid elements. On the other hand, the residual stresses introduced during step 1, were combinations of uniaxial compression (σ_x = -1, σ_y = 0), biaxial compression (σ_x = -1, σ_y = -1) and a combined compression states (σ_x = -1, σ_y = -0.8). All stress units are MPa.

The redistribution of residual stress is shown in Fig. 7 for different mesh sizes and stress states. As reported by Ajovalasit et al. [29] and Beghini et al. [26], plasticity during hole drilling should be taken into account, as equations for strain release just assume elastic material behaviour. However, Ajovalasit et al. [29] showed that for biaxial stress, elastic performance was accurate enough, and plasticity does not imply any meaningful adjustment.

Figure 7

Fig. 8 shows that strain release is positive for compression residual stress, presenting the same results when $\sigma_x = \sigma_y$. On the other hand, the strain release in the x axis increases if the compressive stress in the y direction is lower in magnitude. When compression is a result of the combination of two different stress levels, σ_x = 1 MPa and σ_y = 0.8 MPa, the strain release obtained is within the range 0.82 ± 0.22 μm/m (±26.8%). For a complete uniaxial load, the strain release becomes negative in the *y* direction. On the other hand, results obtained with fine meshes are similar to those obtained with coarse ones, as shown in Fig. 9.

Figure 8

Figure 9

Once simulated the material removal, and strains obtained for each strain gage as a function of the drilling depth, results were combined with the formerly found calibration parameters *a* and *b*, to obtain the direction of main stresses (Eq. 6), and in the *x* (Eq. 7) and y directions (Eq. 8).

$$\theta = \frac{1}{2}\arctan\left(\frac{\Delta\varepsilon_x - 2\Delta\varepsilon_{xy} + \Delta\varepsilon_y}{\Delta\varepsilon_x - \Delta\varepsilon_y}\right) \tag{6}$$

$$\sigma_x = \frac{\Delta\varepsilon_x(a + b\sin 2\theta) - \Delta\varepsilon_y(a - b\cos 2\theta)}{2ab(\sin 2\theta + \cos 2\theta)\Delta h} = E\frac{\Delta\varepsilon_x(a(1+\upsilon) + b\sin 2\theta) - \Delta\varepsilon_y(a(1+\upsilon) - b\cos 2\theta)}{a(1+\upsilon)b(\sin 2\theta + \cos 2\theta)\Delta h}\,[\text{MPa}] \tag{7}$$

$$\sigma_y = \frac{\Delta\varepsilon_y(a + b\sin 2\theta) - \Delta\varepsilon_x(a - b\cos 2\theta)}{2ab(\sin 2\theta + \cos 2\theta)\Delta h} = E\frac{\Delta\varepsilon_y(a(1+\upsilon) + b\sin 2\theta) - \Delta\varepsilon_x(a(1+\upsilon) - b\cos 2\theta)}{a(1+\upsilon)b(\sin 2\theta + \cos 2\theta)\Delta h}\,[\text{MPa}] \tag{8}$$

Where $\Delta\varepsilon$ is the strain gage increment during release, *a* and *b* are the calibration parameters obtained previously, *E* is the material Young's modulus, *v* is the material Poisson's ratio, Θ is the direction of maximum stress, and σ_x and σ_y are the residual stresses calculated in *x* and *y* directions.

Parameters for the RY21 rosette have been calculated and validated using finite element simulations, in the same way as developed in Garcia-Granada et al. [18]. The calculated residual stresses obtained from strain release are plotted in Fig. 10 to confirm that results are accurate, except for the region near the edge of the drill hole. Three simulations were checked considering a biaxial residual stress state (σ_x = -1, σ_y = -1), a uniaxial case (σ_x = -1, σ_y = 0) and a combined case (σ_x = -1, σ_y = -0.8). Equations and parameters were proved to deliver an acceptable value of residual stress calculated from strain release using the incremental hole drilling method.

Figure 10

3. Results and discussion

The incremental hole drilling method was applied on every tested specimen, and results were then registered and corrected with the results obtained by the previously calculated FEM. Results below are shown for one sample of each material.

AISI 2038 results

The microstrain released during the experiment at the steel specimen #5 is shown in figure 11, for the three gauges forming the rosette along the *x*, *y* and *xy* directions. These strains can be compared with the predictions calculated through the FEM analysis, which was shown in Fig. 8. If the results for the $\sigma_y = 0.8\sigma_x$ hypothesis is taken into account, the difference between both results is well below the 26,8% which defines the resulting stress interval, and therefore, can be taken as valid for this experimental setup. This fact shows that ball burnishing introduces residual stresses through a combined stress mechanism, and is far from a uniaxial behavior which might be supposed at first instance. This result makes sense if the ball burnishing performance is taken into account. The tool is programmed so that its feed movement covers the whole surface extension, and, on the other hand, the successive passes along the *x* and *y* axes perform cold deformation processes along both of them.

The results presented have been modified by applying a correction through the *a* and *b* rosette calibration parameters obtained by the second FEM. If these were not considered, residual stress results show similar values on both axes. Steel ball-burnished samples showed an average maximum strain relief of 88 ± 12 μm/m (±13.6%).

Figure 11

The obtained residual stresses were also corrected using eqs. (6), (7) and (8), which take into consideration all corrections done through the FEM. Real residual stresses deduced from those expressions have been plotted for specimen #5, and are shown at Fig. 12 in order to compare them with results obtained on similar materials through X-ray diffraction by Gómez-Gras [44] and Travieso-Rodriguez et al. [15], on superficial layers of the material. This figure evidences the potential of burnishing to induce residual stresses on materials, which in this case could be measured by stepping up on the measuring method. X-ray diffraction provide similar results as IHD at superficial layers, and can be, therefore, equivalently used if only surface residual stress wants to be assessed.

Figure 12

AA2017-T4 results

The same procedure was followed for aluminum specimens, considering the microstrain release in the *x*, *y* and *xy* directions (Fig. 13). In the case of the aluminum specimens, all four tested parts showed a final average maximum strain relief of 139 ± 14 [µm/m] (±10%). That value of dispersion of the residual stress measurements in aluminum samples is similar as the dispersion found in the steel specimens results. However, AA2017-T4 workpieces showed a higher strain relief after burnishing, which means that higher cold working deformation was executed on the aluminum surface due to plasticity burnishing. This is caused by the fact that aluminum is softer than steel, and presents a lower self-hardening coefficient, thus deriving in higher cold work deformation, although a lower burnishing force is applied. Furthermore, as surface deformation is performed by the successive burnishing passes, self-hardening caused by one of them highly influences the next pass, which is to be performed along a different

burnishing path. A low self-hardening coefficient material such as aluminum is due t o be less affected by this effect, and is able to experience more strain.

Figure 13

To transform microstrain values into residual stress, the correcting equations (6), (7) and (8) were considered. Fig. 14 show results for specimen #4, as a relevant example of the aluminum specimens' behavior. On the other hand, results obtained through the X-ray diffraction technique, and reported by Gómez-Gras [44] and by Travieso-Rodríguez et al. [14] on a similar aluminum have been also represented for comparison. X-ray measurement values are coherent with IHD results, and therefore, both methods can be described as equivalent to assess residual stress at surface layers of the aluminum material, as was also concluded for the AISI 2038 specimens.

Figure 14

4. Conclusions

At sight of the results obtained, the following conclusions can be drawn:

(1) The calibration of the RY21 rosette has been developed for a 5 mm hole, and taking steps of 0.05 mm, showing that the approximation proposed by the E837-08 ASTM standard could lead to significant errors when changing the gage length, the hole diameter and the steps between drillings at the same time. This calibration has been verified by an FEM of the IHD process, simulating the strain release of a hypothetical residual stress state.

(2) The residual stresses introduced by a ball-burnishing operation are very similar in the x and y directions, obtaining accurate results through the IHD technique.

(3) Ball burnishing has proved to introduce relevant residual stress up to 0.6 mm depth. This finding justifies the relevance of ball-burnishing as an industrial finishing process, and evidences its potential to finish parts subjected to fatigue working regimes.

(4) Residual stresses near the surface measured by IHD are very similar to the measurements made through the X-Ray diffraction technique. This conclusion, coupled to the fact that IHD technique is cheaper and faster than X-Ray diffraction, positions IHD as a good and feasible alternative to the latter.

Funding / Acknowledgments

Financial support for this study was provided by the Ministry of Economy and Competitiveness of Spain, through grant DPI2015-69803-R, which is greatly appreciated.

References

1. Shepard, N.J.; Michael, J.; Prevéy, P.S. Effects of Surface Treatment on Fretting Fatigue Performance of Ti-6Al-4V; In *Proceedings of the 8th National Turbine Engine High Cycle Fatigue*, Monterey, Canada, Apr 14–16, 2003**.**
2. Yen, Y.C.; Sartkulvanich, P.; Altan, T. Finite Element modeling of roller burnishing process. *CIRP Annals - Manufacturing Technology* **2005**, *54*(1), 237–240. doi:10.1016/S0007-8506(07)60092-4
3. El-Axir, M.H.; Othman, O.M.; Abodiena, A.M. Study on the inner surface finishing of aluminum alloy 2014 by ball burnishing process. *Journal of Engineering Research* **2008**, *202*(1–3), 435–442.
4. Travieso-Rodriguez, J.A.; Dessein, G.; González-Rojas, H.A. Improving the surface finish of concave and convex surfaces using a ball burnishing process. *Materials and Manufacturing Processes* **2011**, *26*(12), 1494–1502.
5. Prevéy, P.S.; Hornbach, D.J.; Jacobs, T.L.; Ravindranath, R. Improved damage tolerance in titanium alloy fan blades with low plasticity burnishing. *Lambda*

Technologies Research Report N68335-01-C-0274, **2002**. Retirved from: http://www.lambdatechs.com/documents/234.pdf. Accessed 19/01/2017

6. Zhang, Q.; Mahfouf, M.; Yates, J.R.; Pinna, C.; Panoutsos, G.; Boumaiza, S; Greene, R.J.; de Leon, L. Modeling and optimal design of machining-induced residual stresses in aluminium alloys using a fast hierarchical multiobjective optimization algorithm. *Materials and Manufacturing Processes* **2011**, *26*(3), 508–520. doi:10.1080/10426914.2010.537421
7. Mahmood Hassan A.; Al-Dhifi, S.Z. Improvement in the wear resistance of brass components by the ball burnishing process. *Journal of Materials Processing Technology* **1999**, *96*(1), 73–80. doi:10.1016/S0924-0136(99)00254-X
8. Hariharan, K.; Prakash, R. V. Integrating effect of forming in fatigue life prediction: review of present scenario and challenges. *Proceedings of the Institution of Mechanical Engineers, Part B: Journal of Engineering Manufacture* **2012**, *226*(6), 967–979.
9. Mech-India Engineers Ltd burnishing tools catalogue. Retrieved from: http://www.mechindia.com/cat/download.htm. Accessed: 19/01/2016.
10. Ecoroll AG Werkzeugtechnik Hydrostatic Tools catalogue. Available: http://www.ecoroll.de/en/products/hydrostatische-werkzeuge.html. Accessed: 19/01/2016.
11. Travieso-Rodriguez, J.A.; Gonzalez-Rojas, H.A.; Casado-Lopez, R. Herramienta con bola a baja presión, aplicable para bruñido de superficies. Spanish Patent Reference P201130331. *Spanish Official Journal of Intellectual Property* **2013**, *21*(11).
12. Rodríguez, A.; López de Lacalle, L.N.; Celaya, A.; Lamikiz, A.; Albizuri, J. Surface improvement of shafts by the deep ball-burnishing technique. *Surface and Coatings Technology* **2012**, *206*(11–12), 2817–2824. doi:10.1016/j.surfcoat.2011.11.045
13. Zhao, J.; Liu, Z. Investigations of ultrasonic frequency effects on surface deformation in rotary ultrasonic roller burnishing Ti-6Al-4V. *Materials & Design* **2016**, *107*, 238–249. doi:10.1016/j.matdes.2016.06.024
14. Travieso-Rodriguez, J.A.; Gómez Gras, G.; Jorba Peiró, J.; Carrillo, F.; Dessein, G.; Alexis, J.; González-Rojas, H.A. Experimental study on the mechanical effects of the vibration-assisted ball-burnishing process. *Materials and*

Manufacturing Processes **2015**, *30*(12), 1490–1497. doi:10.1080/10426914.2015.1019114

15. Travieso-Rodriguez, J.A.; Gómez Gras, G.; Dessein, G.; Carrillo, F.; Alexis, J.; Jorba-Peiro, J.; Aubazac, N. Effects of a ball-burnishing process assisted by vibrations in G10380 steel specimens. *International Journal of Advanced Manufacturing Technology* **2015**, *81*(9-12), 1757–1765. doi:10.1007/s00170-015-7255-3
16. Withers, P. J.; Bhadeshia, H.K.D.H. Residual stress. Part 1–measurement techniques. *Materials Science and Technology* **2001**, *17*(4), 355–365.
17. Withers, P. J.; Bhadeshia, H.K.D.H. Residual stress. Part 2–Nature and origins. *Materials Science and Technology* **2001**, *17*(4), 366–375.
18. Garcia-Granada, A.A.; Smith, D.J.; Pavier, M.J. A new procedure based on Sachs' boring for measuring non-axisymmetric residual stresses. *International Journal of Mechanical Sciences* **2000**, *42*(6), 1027–1047. doi:10.1016/S0020-7403(99)00039-9
19. Garcia-Granada, A.A.; Lacarac, V.D.; Smith, D.J.; Pavier, M.J. A new procedure based on Sachs' boring for measuring non-axisymmetric residual stresses: Experimental application. *International Journal of Mechanical Sciences* **2001**, *43*(12), 2753–2768. doi:10.1016/S0020-7403(01)00071-6
20. Hossain, S.; Truman, C.E.; Smith, D.J. Finite element validation of the deep hole drilling method for measuring residual stresses. *International Journal of Pressure Vessels and Piping* **2012**, *93*, 29–41. doi:10.1016/j.ijpvp.2012.02.003
21. Garcia-Granada, A.A.; George, D.; Smith, D.J. Assessment of distortions in the deep hole technique for measuring residual stress; In *Proceedings of the 11th conference on experimental mechanics*, Oxford, Great Britain, Aug 24–28, 1999; Allison, I.M, et al. Eds.,: Brookfield: Rotterdam,1998.
22. Maawad, E.; Brokmeier, H.G.; Hofmann, M.; Genzel, C.; Wagner, L. Stress distribution in mechanically surface treated Ti-2.5Cu determined by combining energy-dispersive synchrotron and neutron diffraction. *Materials Sciences and Engineering: A* **2010**, *527*(21), 5745–5749. doi: 10.1016/j.msea.2010.05.044
23. Prevéy, P.S.; Cammett, J. Low Cost Corrosion Damage Mitigation and Improved Fatigue Performance of Low Plasticity Burnished 7075-T6. *Journal of Materials Engineering and Performance* **2001,** *10*(5), 548–555. doi:10.1361/105994901770344692

24. Noyan, I.C.; Cohen, J.B. *Residual stress: measurement by diffraction and interpretation*; Springer Science+Business Media: New York, USA, 2013.
25. Kumar, A.; Welzel, U.; Mittemeijer, E.J. A method for the non-destructive analysis of gradients of mechanical stresses by X-ray diffraction measurements at fixed penetration/information depths. *Journal of Applied Crystallography* **2006**, *39*(5), 633–646. doi:10.1107/S0021889806023417
26. Beghini, M.; Santus, C.; Valentini, E.; Benincasa, A. Experimental verification of the hole drilling plasticity effect correction. *Materials Science Forum* **2011,** *681*, 151–158. doi:10.4028/www.scientific.net/MSF.681.151
27. Sedighi, M.; Mahmoodi, M. Experimental and numerical study of through thickness residual stresses distribution in sheet metals produced by ECAR. *International Journal of Advanced Design and Manufacturing Technology* **2012,** *5*(4), 71–76.
28. American Society for Testing and Materials. Standard test method for determining residual stresses by the hole drilling strain gage method. Standard No. E937-08, 2008.
29. Ajovalasit, A.; Scafidi, M.; Zuccarello, B.; Beghini, M.; Bertini, L.; Santus, C.; Valentini, E.; Benincasa, A.; Bertelli, L. Il metodo di prova "AIAS - TR" per la misura delle tensioni residue costanti o variabili con la tecnica del foro incrementale. In *Proceedings of the XXXIX National Congress of the Italian Association for the analysis of solicitations*, Maratea, Italy, Sept 7–10, 2010. Retrieved from
30. Beghini, M.; Santus, C.; Valentini, E.; Benincasa, A. Experimental verification of the hole drilling plasticity effect correction. *Materials Science Forum* **2011,** 681, 151–158. doi:10.4028/www.scientific.net/MSF.681.151
31. Mahmoudi, A.H.; Truman, C.E.; Smith, D J.; Pavier, M.J. The effect of plasticity on the ability of the deep hole drilling technique to measure axisymmetric residual stress. *International Journal of Mechanical Sciences* **2011** *53*(11), 978–988. doi:10.1016/j.ijmecsci.2011.08.002
32. Ficquet, X.; Hedmar, M; Kingston, E.J. Residual stress measurement in an ultrasonic peened specimen. In *Proceedings of 33rd International Conference on Ocean, Offshore and Arctic Engineering, Volume 5: Materials Technology; Petroleum Technology*, San Francisco, California, June 8–13, 2014. doi:10.1115/OMAE2014-23374

33. Gharbi, F.; Sghaier, S.; Morel, F.; Benameur, T. Experimental investigation of the effect of burnishing force on service properties of AISI 1010 steel plates. *Journal of Materials Engineering and Performance* **2015**, *24*(2), 721–725. doi:10.1007/s11665-014-1349-1
34. Zemčík, O.; Chladil, J; Sedlák, J. Changes in the surface layer of rolled bearing steel changes in the surface layer of rolled. *Acta Polytechnica* **2015,** *55*(5), 347–351. doi:10.14311/AP.2015.55.0347
35. Abdulstaar, L. W. M.; Mhaede, M.; Wollmann, M. Effects of shot peening and ball-burnishing on the fatigue performance of Al 6082. In *Proceedings of the 12th International Conference on Shot Peening*, Goslar, Germany, Sept 15–18, 2014.
36. Gómez-Gras, G.; Travieso-Rodriguez, J.A.; González-Rojas, H.A.; Nápoles-Alberro, A.; Carrillo, F.; Dessein, G. Study of a ball-burnishing vibration-assisted process. *Proceedings of the Institution of Mechanical Engineers, Part B: Journal of Engineering Manufacture* **2015**, *229*(1), 172–177. doi:10.1177/0954405414526383
37. Schajer, G.S.; Steinzig, M. Full-field calculation of hole drilling residual stresses from electronic speckle pattern interferometry data. *Experimental Mechanics* **2005,** *45*(6), 526–532. doi:10.1007/BF02427906
38. Montay, G.; Cherouat, A.; Lu, J. Incremental hole drilling and X-ray diffraction techniques to the residual stresses determination introduced by shot peening in titanium alloy. *Journal of Neutron Research* **2001**, *9*(2–4), 337–344.
39. Niku-Lari, A.; France, IITT. An overview of Shot Peening. In *Proceedings of* the *International Conference on Shot Peening and Blast Cleaning,* 1996.
40. Xiao, B.; Li, K.; Rong, Y. Numerical study on calibration coefficients for hole-drilling residual stress measurement. In *Proceedings of the SEM Annual Conference*, Alburquerque, Mexico, Jun 1–4, 2009; Society for Experimental Mechanics, Pub.: Curran Asociates Ltd.: New York, 2009.
41. Svarıcek, K.; Vlk, M. Residual stress evaluation by the hole-drilling method with eccentric hole. *Engineering Mechanics* **2007,** *14*(3), 191–197.
42. Ghasemi, A. R.; Mohammadi, M.M. Residual stress measurement of fiber metal laminates using incremental hole-drilling technique in consideration of the integral method. *International Journal of Mechanical Sciences* **2016**, *114*, 246–256. doi:10.1016/j.ijmecsci.2016.05.025

43. Schuster, S.; Gibmeier, J. Incremental hole drilling for residual stress analysis of strongly textured material states–a new calibration approach. *Experimental Mechanics* **2016**, *56*(3), 369–380. doi:10.1007/s11340-015-0104-3
44. Gomez-Gras G. Estudio del proceso de bruñido con bola asistido por una vibración. PhD dissertation, Universitat Politècnica de Catalunya, Spain, 2013.

Figure 1. Ball-burnishing tool used in the experiments. A) Schematic representation. B) Real device.

Figure 2. A) 1-RY21-3/120 strain gage rosette set up on a ball-burnished specimen. B) Fixation of specimen on Odisea CNC with controller Fagor 8055 for incremental hole drilling.

Figure 3. Parametric model in SOLIDWORKS to obtain a and b parameters

Figure 4. Fitted curve for the estimation of a and b parameters as a function of the depth

Figure 5. Device to perform the 4-point bending test, to validate the residual stress measurements

Figure 6. Experimental validation of the stress calculation through the developed strain gage method

Figure 7. Residual stress distribution during hole drilling for A) uniaxial stress with initial coarse mesh, B) biaxial stress with intermediate mesh size and C) combined stress state $\sigma x = -1$, $\sigma y = -0.8$) for fine mesh.

Figure 8. Microstrains release obtained with FEM simulations and coarse mesh for three different initial residual stress states

Figure 9. Microstrains release obtained with FEM simulations, for elements derived from a coarse mesh and a maximum depth of 5 mm compared to a fine mesh up to 2 mm depth

Figure 10. Residual stress calculation from FEM strain release to validate parameters a and b for the RY21 rosette

Figure 11. Experimental microstrain release from the four ball-burnished steel samples

Figure 12. Residual stress as a function of depth for steel sample #5, and compared with the results of X-ray measurements obtained by Travieso-Rodríguez et al. [14] and Gómez-Gras [41]

Figure 13. Microstrain experimental relief for the four different ball-burnished aluminum samples

Figure 14. Residual stress as a function of depth for aluminum sample #4 and compared with the results of X-ray measurements shown in Travieso-Rodríguez et al. [13] and Gómez-Gras [41]

Table 1. Properties of materials used for both workpieces

Table 1. Properties of materials used for both workpieces

Material	δ [kg/m^3]	σ_y [MPa]	σ_u [MPa]	ε_f [%]	E [GPa]	ν[-]
2017-T4 aluminium	2.8	275	427	22	72.4	0.33
AISI 2038 steel	7.8	285	515	18	200	0.29

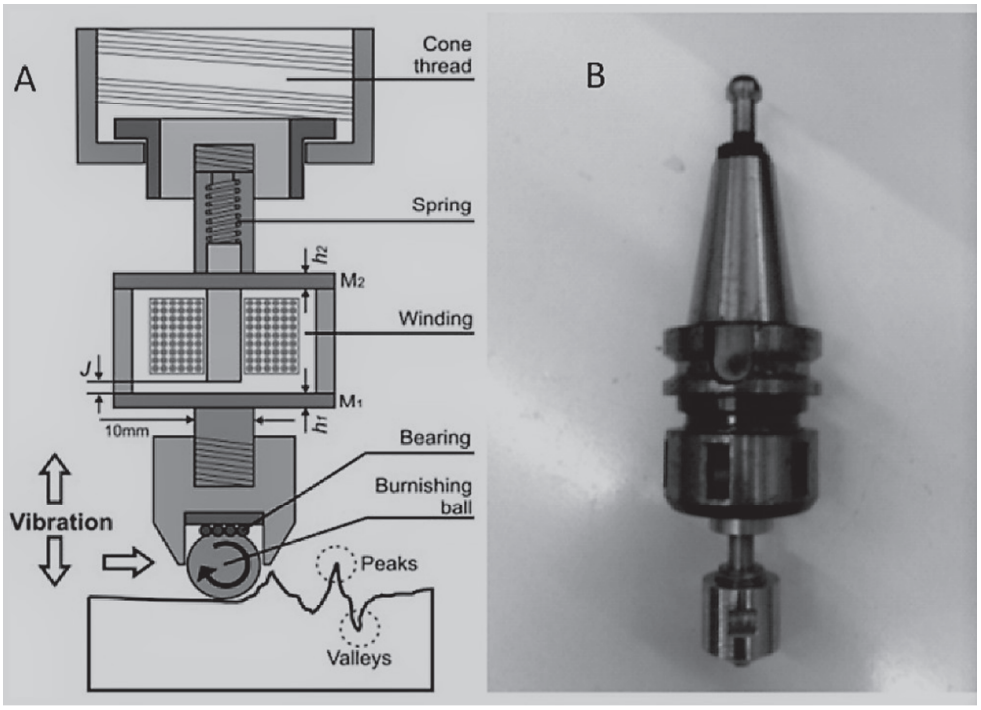

Figure 1. Ball burnishing tool used in the experiments. A) Schematic representation. B) Real device
Fig. 1
84x60mm (300 x 300 DPI)

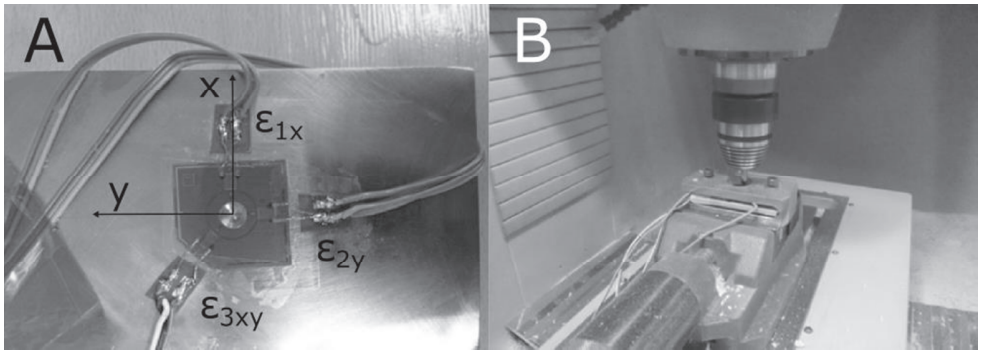

Figure 2. A) 1-RY21-3/120 strain gage rosette set up on a ball-burnished specimen. B) Fixation of specimen on Odisea CNC with controller Fagor 8055 for incremental hole drilling
Fig. 2
84x30mm (299 x 299 DPI)

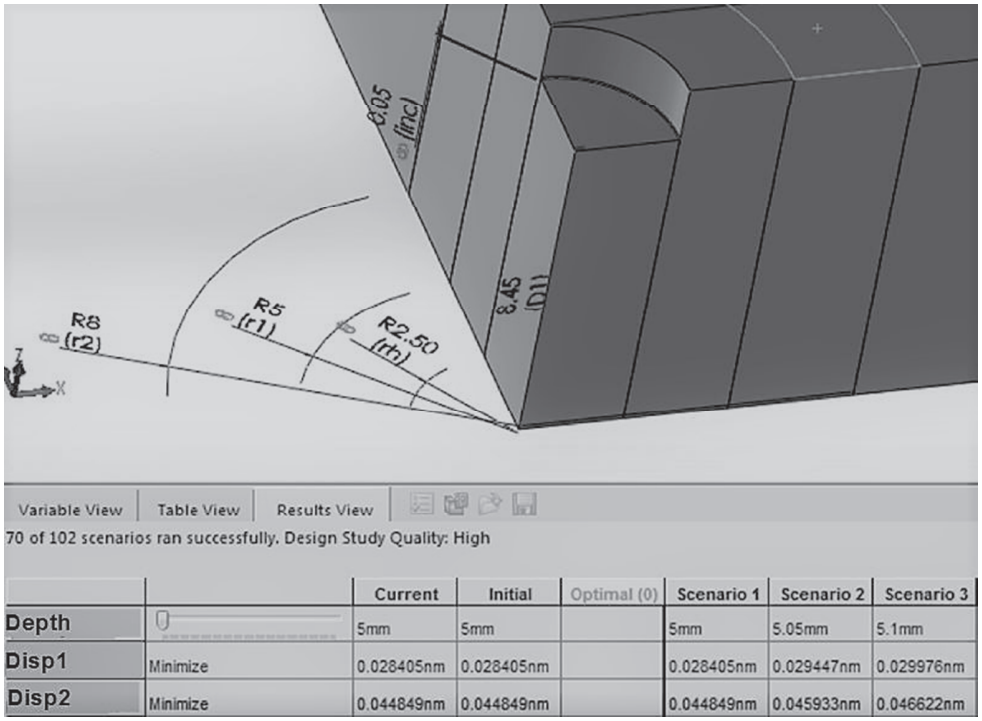

Variable View | Table View | Results View

70 of 102 scenarios ran successfully. Design Study Quality: High

		Current	Initial	Optimal (0)	Scenario 1	Scenario 2	Scenario 3
Depth		5mm	5mm		5mm	5.05mm	5.1mm
Disp1	Minimize	0.028405nm	0.028405nm		0.028405nm	0.029447nm	0.029976nm
Disp2	Minimize	0.044849nm	0.044849nm		0.044849nm	0.045933nm	0.046622nm

Figure 3. Parametric model in SOLIDWORKS to obtain a and b parameters
Fig. 3
211x155mm (96 x 96 DPI)

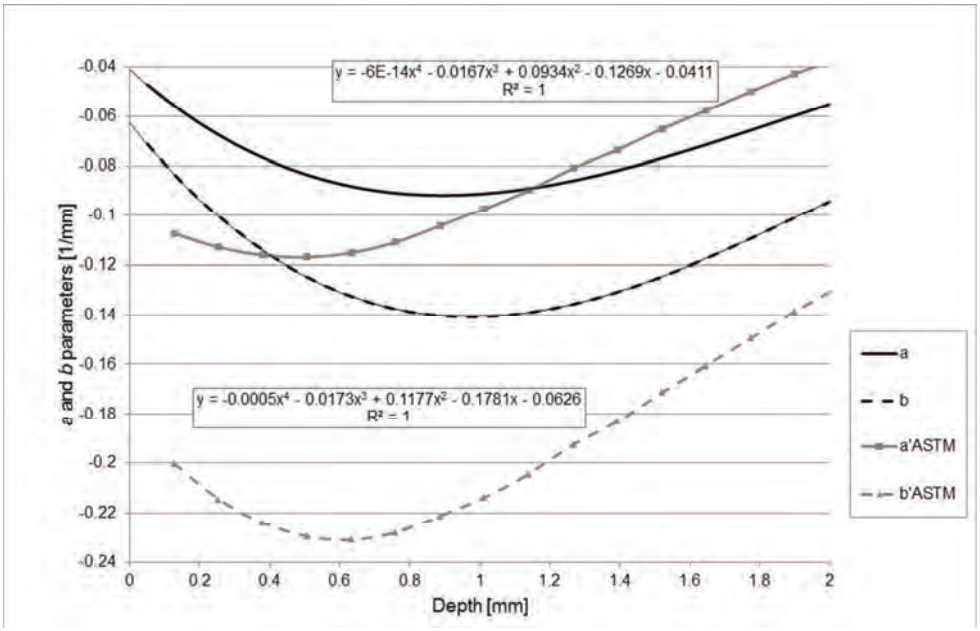

Figure 4. Fitted curve for the estimation of a and b parameters as a function of the depth
Fig. 4
82x53mm (300 x 300 DPI)

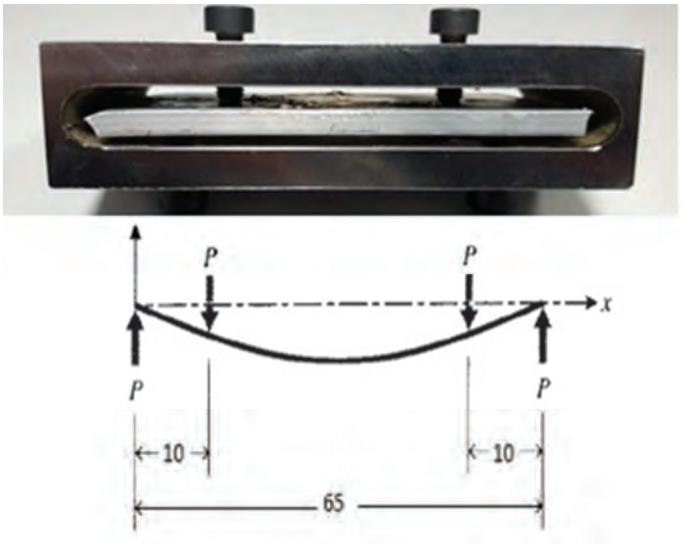

Figure 5. Device to perform the 4-point bending test, to validate the residual stress measurements
Fig. 5
92x73mm (96 x 96 DPI)

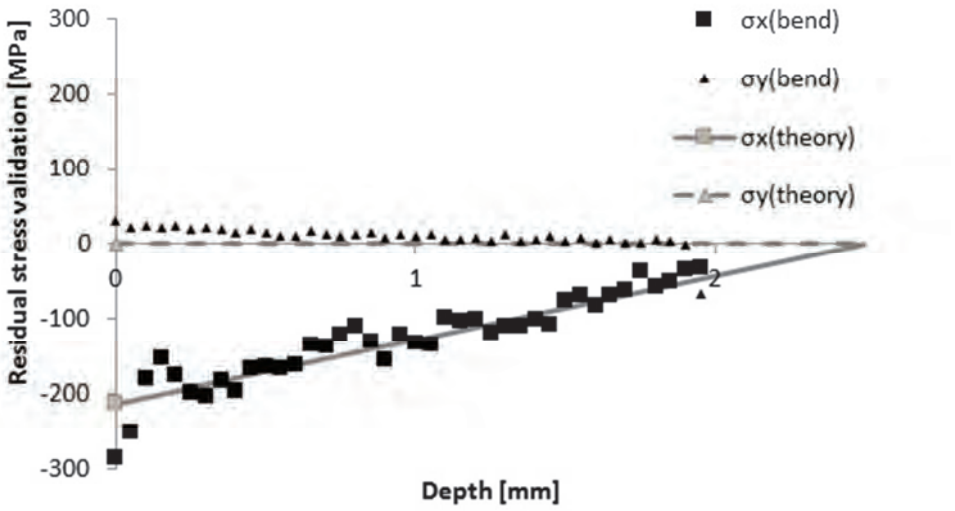

Figure 6. Experimental validation of the stress calculation through the developed strain gage method
Fig. 6
150x80mm (96 x 96 DPI)

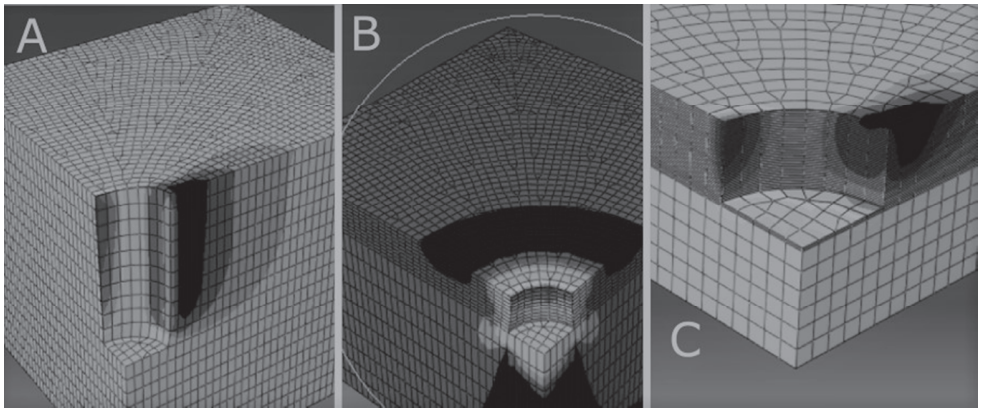

Figure 7. Residual stress distribution during hole drilling for A) uniaxial stress with initial coarse mesh, B) biaxial stress with intermediate mesh size and C) combined stress state σx = -1, σy = -0.8) for fine mesh.
Fig. 7
76x31mm (300 x 300 DPI)

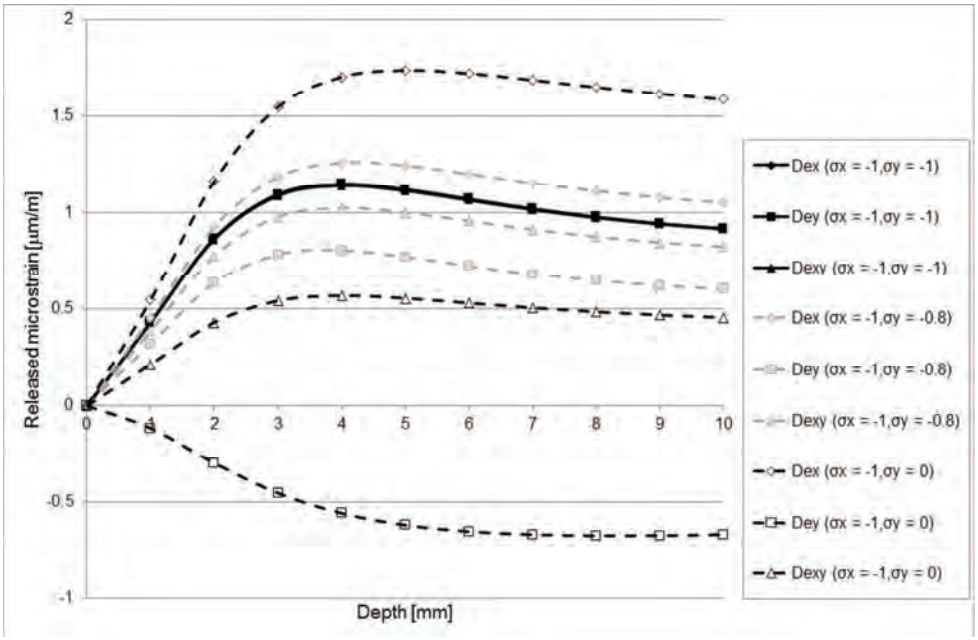

Figure 8. Microstrains release obtained with FEM simulations and coarse mesh for three different initial residual stress states
Fig. 8
82x53mm (300 x 300 DPI)

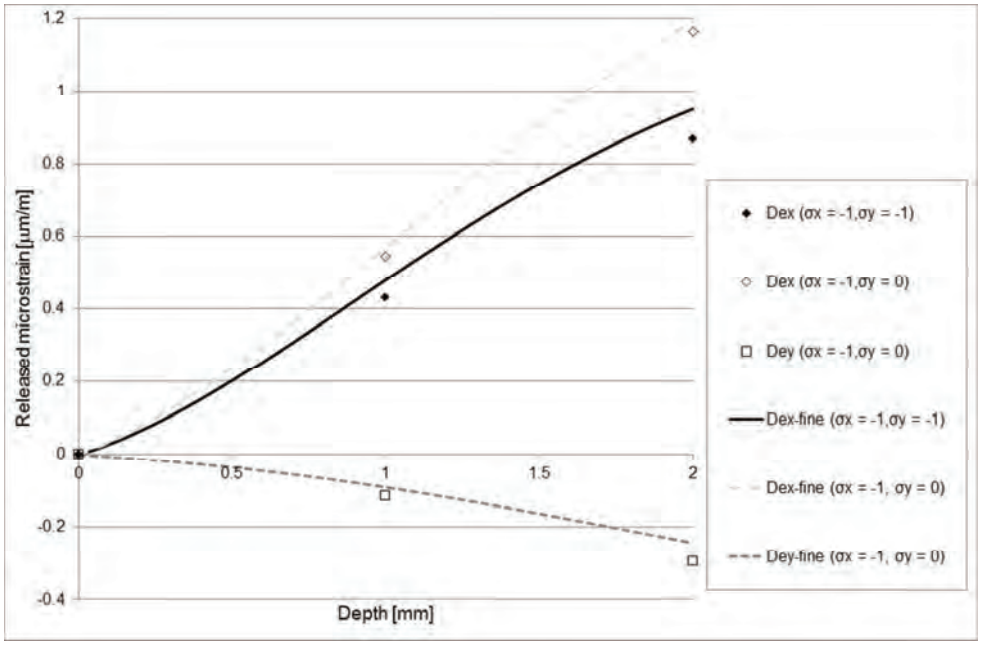

Figure 9. Microstrains release obtained with FEM simulations, for elements derived from a coarse mesh and a maximum depth of 5 mm compared to a fine mesh up to 2 mm depth
Fig. 9
82x54mm (300 x 300 DPI)

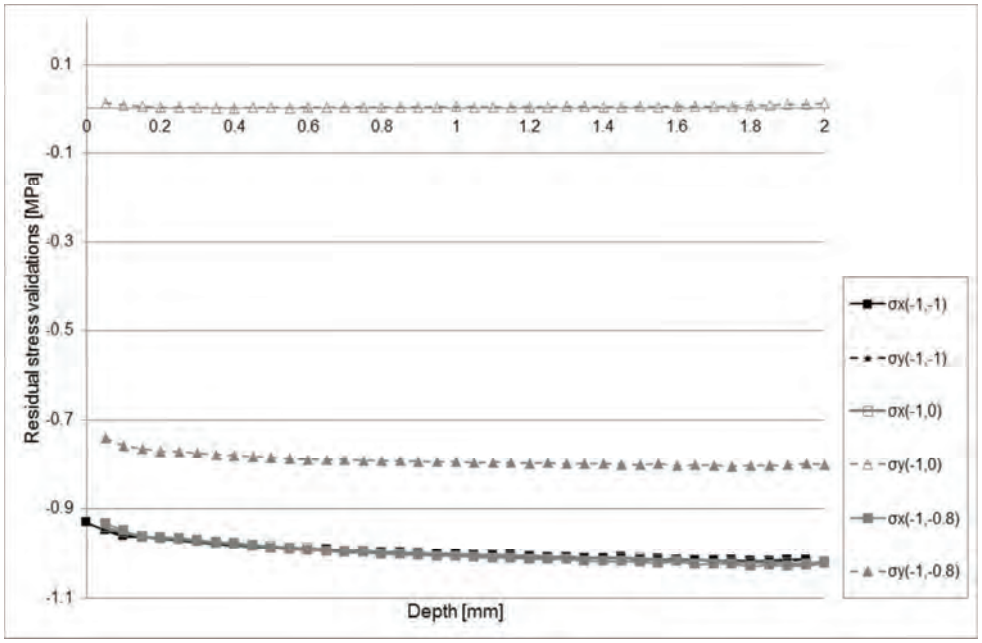

Figure 10. Residual stress calculation from FEM strain release to validate parameters a and b for the RY21 rosette
Fig. 10
82x54mm (300 x 300 DPI)

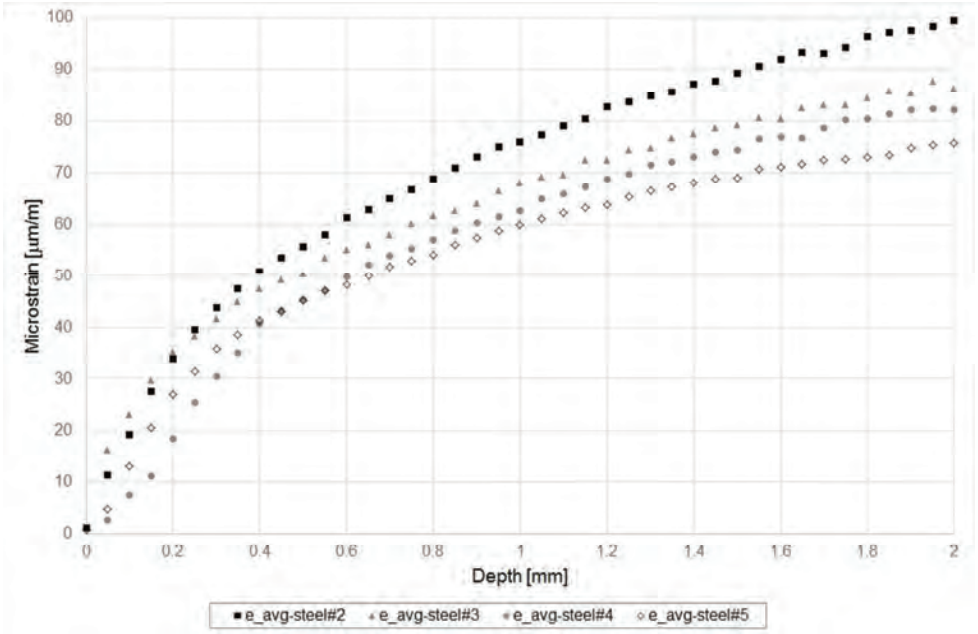

Figure 11. Experimental microstrain release from the four ball-burnished steel samples
Fig. 11
82x53mm (300 x 300 DPI)

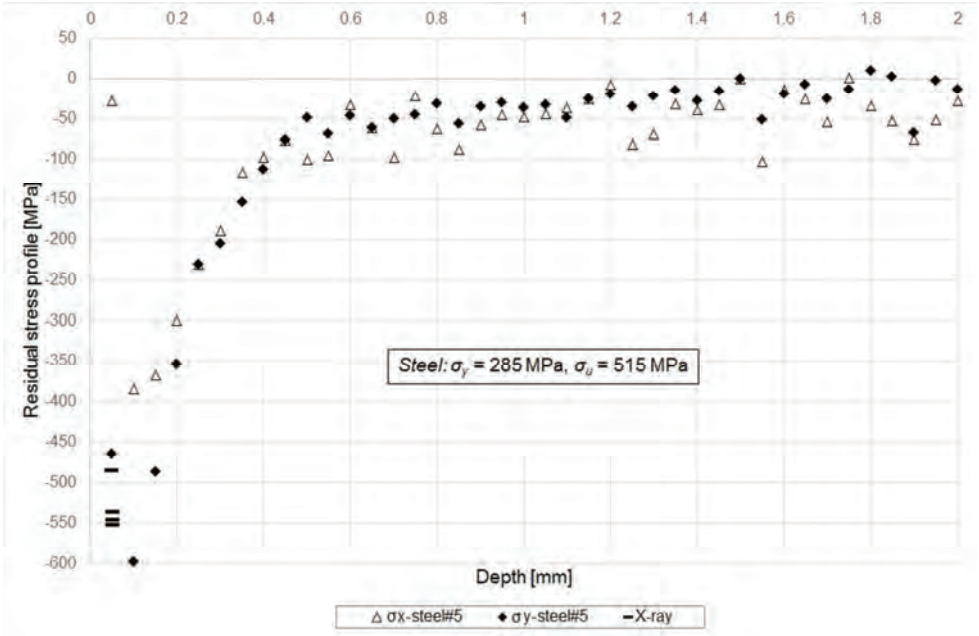

Figure 12. Residual stress as a function of depth for steel sample #5, and compared with the results of X-ray measurements obtained by Travieso-Rodríguez et al. [14] and Gómez-Gras [41]
Fig. 12
82x53mm (300 x 300 DPI)

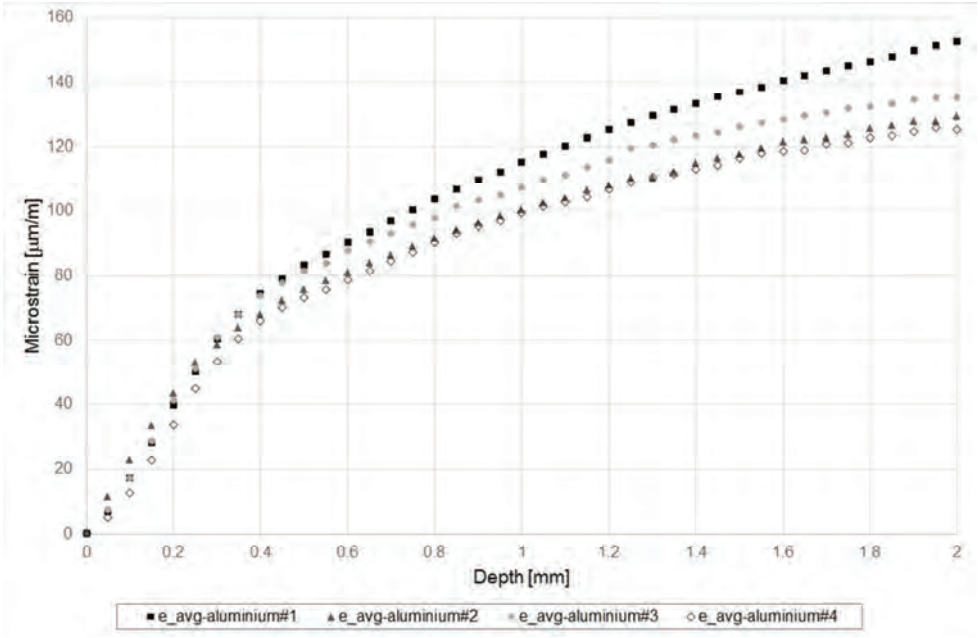

Figure 13. Microstrain experimental relief for the four different ball-burnished aluminum samples
Fig. 13
82x53mm (300 x 300 DPI)

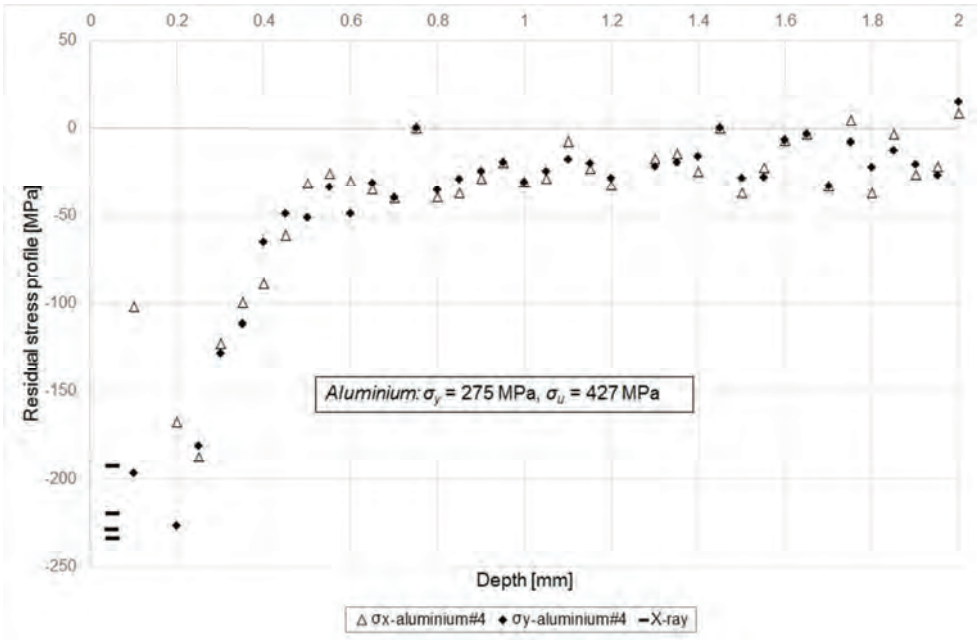

Figure 14. Residual stress as a function of depth for aluminum sample #4 and compared with the results of X-ray measurements shown in Travieso-Rodríguez et al. [13] and Gómez-Gras [41]
Fig. 14
82x54mm (300 x 300 DPI)